A Calphad assessment of Al–C–Fe system with the carbide modelled as an ordered form of the fcc phase

Damien Connétable, Jacques Lacaze, Philippe Maugis, Bo Sundman

A Calphad assessment of Al–C–Fe system with the κ carbide modelled as an ordered form of the fcc phase

Damien Connetable[a], Jacques Lacaze[a], Philippe Maugis[b], Bo Sundman[a,*]

[a] *CIRIMAT, UPS/INPT/CNRS ENSIACET, 31077 Toulouse, France*
[b] *Arcelor Research SA, BP 30320, 57283 Maizières-lès-Metz, France*

Abstract

As part of an extensive study devoted to the development of new high-Al steels, a CALPHAD-type assessment of the Al–Fe–C system has been carried out. In place of the usual cementite, these steels show precipitation of the so-called κ carbide that is an ordered form of austenite. Inconsistencies between the scarce experimental information in the Al–Fe–C system and extrapolations from the available Al–Fe and Al–C descriptions made it necessary to revise them. This has been done in part by using new *ab initio* calculations as well as phase diagram data. The κ carbide has been described as an ordered form of the fcc phase, with its Gibbs energy calculated as the sum of a disordered and an ordered contribution. The additional parameters needed to express the ordered part were evaluated using phase equilibria information and new *ab initio* data related to the κ carbide. With this approach, addition of new alloying elements, like Mn or Ni, for extrapolation to higher-order systems should be straightforward.

Keywords: Computational thermodynamics; *Ab initio*; Alloys; Phase diagram; Al–C–Fe

1. Introduction

The ternary system Al–C–Fe has interesting properties for a new class of high-Al steels. Addition of carbon to Al–Fe expands the fcc region (also called austenite or γ and with Strukturbericht designation A1) in the ternary system and there is a cubic carbide called κ, with the Strukturbericht $E2_1$, which can form a eutectoid structure with bcc (also called ferrite and with Strukturberict A2) in the same way as cementite when austenite is cooled. The $E2_1$ structure, also known as perovskite, is an ordered $L1_2$ structure based on the fcc lattice with Al at the cube corners and Fe on the cube faces and a carbon atom in the central octahedral site.

The Al–C–Fe system has previously been assessed with the Calphad method and using *ab initio* data by Ohtani et al. [28]. They took into account the similarity of the $L1_2$ and the κ carbide but the extended austenite region in the ternary system and the solubility range of the κ carbide were not well described. Furthermore, their results from *ab initio* calculations were found to differ considerably from similar data reported in the literature and thus new calculations were performed for the present study.

Using available assessments for the three binary systems it was found that the extrapolations gave too small solubility of Al in the austenite. As explained below this could not be described by any ternary parameter without a modification of the thermodynamic model parameters for the fcc phase in Al–Fe and Al–C. *Ab initio* calculations of the metastable ordered and disordered fcc phase in Al–Fe and for a metastable cubic AlC carbide were made to improve the reliability of these extrapolations. The use of *ab initio* data for Calphad assessments is further discussed in [37]. A Calphad description of the whole system including the κ carbide has been assessed which is compatible with the existing multicomponent databases [35].

2. Lower-order systems

The Al–C system has been assessed by Gröbner et al. [21], the Al–Fe by Seiersten [19] and revised by Ohnuma [25] and

* Corresponding author.
E-mail address: bosse@mse.kth.se (B. Sundman).

doi:10.1016/j.calphad.2008.01.002

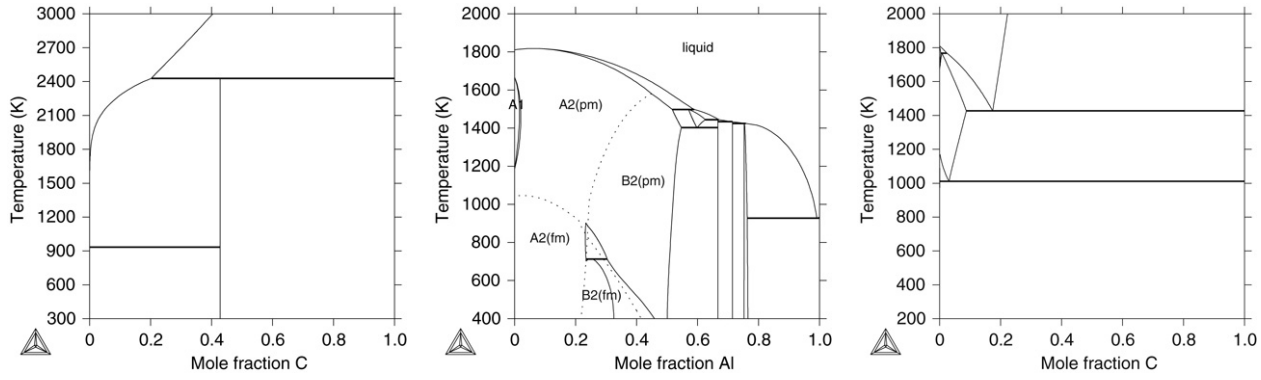

(a) Al–C. (b) Al–Fe. (c) Fe–C.

Fig. 1. Binary phase diagrams. For the Al–Fe diagram the second-order transition between A2 (bcc) and B2 (ordered bcc) and between paramagnetic (pm) and ferromagnetic (fm) regions are dashed. See the text for more details.

the C–Fe system by Gustafson [11]. The calculated phase diagrams are shown in Fig. 1 and in the Al–Fe diagram the dashed lines represent the second-order ferromagnetic ordering and the chemical ordering between A2 and B2. The more complex bcc ordering with Strukturbericht $D0_3$ has not been included in the model and the diagram is thus not correct below 800 K on the Fe-rich side.

As explained below the binary systems Al–C and Al–Fe were partially re-investigated for several reasons. Such modifications should not change the stable binary systems unless there are new data and one must also check that there are no unexpected effects in ternary or higher-order systems that have been assessed using the original binary.

The models used for the different phases are discussed in Section 3 as they were selected in function of the extrapolation into the ternary system. See this section for an explanation of the notation for the different parameters used also in this section. For a comprehensive discussion of thermodynamic modelling see Lukas et al. [34].

2.1. Revision of the Al–C system

In the Al–C assessment by Gröbner et al. [21] the solid fcc-Al phase was never investigated and the parameters for this phase found in most databases have been invented without checking the experimental data. The same is true for the parameters of the bcc phase, which is not stable in this binary system.

The solubility of C in Al has been reported to be around 0.03 at.% by Shunk et al. [8]. The Gibbs energy of formation of a metastable cubic AlC carbide with B1 structure was calculated by *ab initio* to be 40 500 J/mol atom, as described in Appendix. A regular solution parameter was then fitted to the experimental solubility. The new parameters for the fcc phase are:

$$G^{\mathrm{fcc}}_{\mathrm{Al:C}} - G^{\mathrm{fcc}}_{\mathrm{Al}} - G^{\mathrm{graphite}}_{\mathrm{C}} = 81\,000 \quad (1)$$

$$L^{\mathrm{fcc}}_{\mathrm{Al:C,Va}} = -80\,000 + 8T. \quad (2)$$

Additionally the parameters for the metastable bcc phase with all interstitial sites filled with carbon were changed from zero to be of the same order of magnitude as that for bcc iron and the interaction parameter was fitted to the maximum solubility of C in bcc at 1473 K in Al–C–Fe from Palm and Inden [20].

$$G^{\mathrm{bcc}}_{\mathrm{Al:C}} - G^{\mathrm{fcc}}_{\mathrm{Al}} - 3G^{\mathrm{graphite}}_{\mathrm{C}} = 100\,000 + 80T \quad (3)$$

$$L^{\mathrm{bcc}}_{\mathrm{Al:C,Va}} = 130\,000 + 14T. \quad (4)$$

These changes do not influence the phase diagram in Fig. 1(a) but the temperature for 3-phase equilibrium liquid +fcc + Al_4C_3 changes from 933.47 K to 933.58 K.

Ohtani et al. [28] had also revised the Al_4C_3 phase in this system but the heat capacity for their description differs considerably from that assessed by Gröbner et al. [21] above 1500 K. In this work it was judged that the experimental information from the ternary Al–C–Fe did not support any modification of the description of the Al_4C_3 phase.

2.2. Revision of the Al–Fe system

The assessment by Seiersten [19] has been used for more than a decade with good results for many calculations of Al-based alloys. The B2-ordered phase in the Fe-rich side was not of primary importance in the original assessment and a revision of parameters for the B2 and $D0_3$ ordering, including the magnetic parameters, has been made by Ohnuma [25]. In order to be compatible with the B2 ordering in the Al–Ni system substitutional vacancies were added by Dupin [26] but this has no influence on the stable phase diagram.

In the ternary Al–C–Fe system some tie-lines for fcc + bcc and fcc + graphite were measured by Palm and Inden [20] and in Fig. 2(a) the extrapolation from the binaries at 1473 K is shown together with three experimental tie-lines. The directions of the calculated tie-lines are good but the carbon content of the fcc phase in equilibrium with bcc is almost double that of the experimental value. A ternary parameter in fcc can increase its stability and the solubility of Al in fcc in equilibrium with bcc and thus decrease the carbon content. But it will also increase the solubility of C in fcc in equilibrium with graphite and that solubility should decrease according to the third experimental tie-line between fcc and graphite. To increase the solubility of Al in fcc along the Al–Fe side the most important parameters are the binary interactions for fcc in Al–Fe. These have been fitted to describe the small solubility of Al in fcc-Fe and the

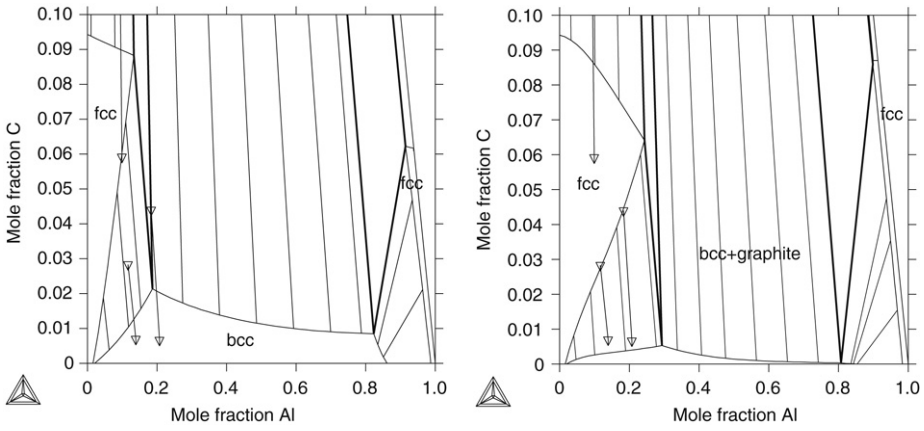

(a) The extrapolation using original Al–C and Al–Fe binaries.

(b) The extrapolation using revised Al–C and Al–Fe binaries.

Fig. 2. Ternary extrapolations at 1473 K using the old (left) and new (right) binaries for Al–C and Al–Fe. Two experimental ternary tie-lines between fcc and bcc from [20] and one between fcc and graphite are included. The fcc, bcc and graphite phases only were considered.

even smaller solubility of Fe in fcc-Al only. Thus there are reasons to believe that the Gibbs energy for the metastable fcc phase relative to the stable bcc phase at higher Al contents is not correctly described in the assessment by Seiersten [19].

It is possible to change the description of the fcc phase in the binary Al–Fe with almost no changes to the stable binary diagram. For such a change it is useful to have *ab initio* calculations of the metastable fcc and also compare with other systems based on the Al–Fe binary with extended solubility of Al in fcc, for example the Al–Fe–Ni and Al–Fe–Mn systems. Changes must be made with great care as they lead to modifications in several higher-order systems. *Ab initio* calculations of the Al–Fe system should be considered with some criticism because they show that the ordered $L1_2$ phase, based on the fcc lattice, should be more stable than the ordered $D0_3$ phase although in reality $D0_3$ is the stable phase at low temperatures around 25 at.% Al. However, modelling the $D0_3$ is outside the scope of this work.

New *ab initio* calculations have been made in this study in order to describe better the stability of the ordered and disordered fcc phase. The values are shown in Table 1 for the ordered forms of fcc and the B2 phases and in Table 2 for the disordered fcc and bcc phases. The methods of the new calculations are described in the Appendix. As can be seen there is a wide range of calculated values for the same structure by different authors due to different approximations made in the calculations, for example the values by Watson [23] do not include the magnetic properties of Fe. When using *ab initio* data in an assessment they should thus be treated as experimental data with reasonable error estimates.

Using these data together with the experimental data for the stable fcc phase in the binary, i.e. the γ-loop close to pure Fe and the solubility of Fe in solid Al, a new set of interaction parameters of the disordered fcc phase was assessed:

$$
\begin{aligned}
{}^0L^{\mathrm{fcc}}_{\mathrm{Al,Fe:Va}} &= -1047\,000 + 30.65T \\
{}^1L^{\mathrm{fcc}}_{\mathrm{Al,Fe:Va}} &= 22\,600 \\
{}^2L^{\mathrm{fcc}}_{\mathrm{Al,Fe:Va}} &= 29\,100 - 13T.
\end{aligned} \tag{5}
$$

Table 1
Ab initio calculated enthalpies of formation of ordered Al–Fe alloys and Calphad type assessed values for the $L1_2$, $L1_0$ and B2 structures

Structure	Mole fraction Al	Enthalpy (kJ/mol atom)	Reference
$L1_2$	0.25	−15.3	LDA [31]
$L1_2$	0.25	−16.7	GGA [31]
$L1_2$	0.25	−16.3	LAG [31]
$L1_2$	0.25	−18.0	[33]
$L1_2$	0.25	−3.9	[23]
$L1_2$	0.25	−19.3	[30]
$L1_2$	0.25	−21.4	[36]
$L1_2$	0.25	−8.8	[28]
$L1_2$	0.25	−19.3	Assessed, this work
$L1_0$	0.5	−16.4	[23]
$L1_0$	0.5	−26.0	[30]
$L1_0$	0.5	−25.9	Assessed, this work
B2	0.5	−31.5	[36]
B2	0.5	−32.9	[30]
B2	0.5	−32.0	Assessed [19]
$L1_2$	0.75	−14.5	[23]
$L1_2$	0.75	−10.2	[30]
$L1_2$	0.75	−10.9	[36]
$L1_2$	0.75	−16.9	[28]
A1	0.75	−14.3	Assessed, this work

The values for B2 are included for comparison.

These regular solution parameters describe an fcc phase without long-range order but include a short-range order (sro) contribution. It is possible to calculate the mixing enthalpy of an fcc phase without sro using *ab initio* techniques as described by Zunger et al. [14]. These can be compared with the excess Gibbs energy in the disordered fcc phase with the sro contribution removed according to an approximation by Abe and Sundman [29]:

$$
\begin{aligned}
{}^0L^{\mathrm{no-sro}}_{\mathrm{Al,Fe:Va}} &= -104\,700 + 30.65T + 1.5u_{\mathrm{AlFe}} \\
{}^1L^{\mathrm{no-sro}}_{\mathrm{Al,Fe:Va}} &= 22\,600 \\
{}^2L^{\mathrm{no-sro}}_{\mathrm{Al,Fe:Va}} &= 29\,100 - 13T - 1.5u_{\mathrm{AlFe}}
\end{aligned} \tag{6}
$$

$$
u_{\mathrm{AlFe}} = -4000 + T, \tag{7}
$$

Table 2
Ab initio calculated values by Connetable et al. [36] for disordered bcc and fcc compared with values from the assessed Al–Fe system

Mole fractions		Structure	E_f	E_f	Assessed value
Al	Fe		(meV/atom)	(kJ/mol atom)	(kJ/mol atom)
1	0	A1	0	0	0
1	0	A2	93.7	9.0	47.5
0.833333	0.166667	A1	−81.8	−7.9	−9.3
0.75	0.25	A1	−105.0	−10.1	−14.1
0.75	0.25	A2	−160.6	−15.6	−12.9
0.666667	0.333333	A1	−151.5	−14.6	−18.2
0.5	0.5	A1	−203.3	−19.6	−22.2
0.5	0.5	A2	−180.6	−17.4	−23.1
0.333333	0.666667	A1	−184.1	−17.7	−18.9
0.25	0.75	A1	−152.9	−14.7	−14.3
0.25	0.75	A2	−148.3	−14.3	−20.3
0.166667	0.833333	A1	−116.6	−11.2	−8.2
0	1	A1	152.0	14.7	8.0
0	1	A2	0	0	0

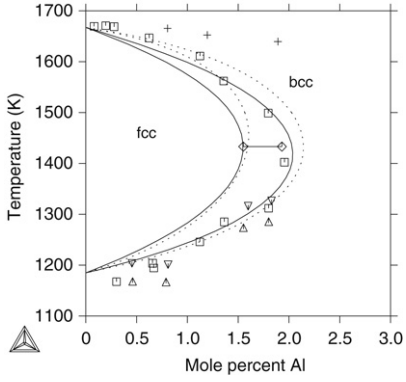

(a) The γ-loop in Al–Fe. The loop assessed by Seiersten is short dashed. Experimental data from [1,2,6].

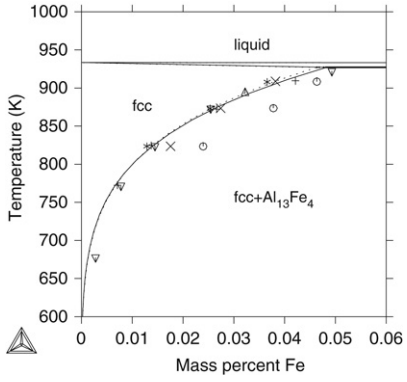

(b) The solubility of Fe in Al, the curve is identical to the previous assessments. Experimental data from [3,4,13].

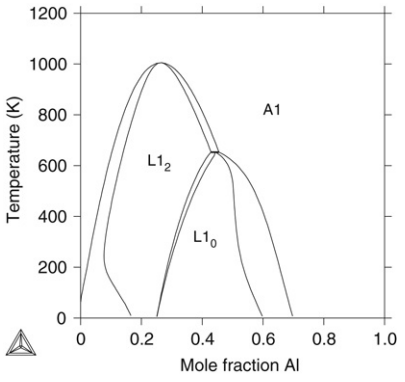

(c) The metastable fcc-ordered phase diagram for Al–Fe. There is no ordered $L1_2$ phase on the Al-rich side.

Fig. 3. The stable and metastable fcc regions in Al–Fe.

where u_{AlFe} represents the average bond energy between Al and Fe in the fcc tetrahedron describing the long-range order. This is used for the Gibbs energies of the ordered end members:

$$
\begin{aligned}
{}^{o}G^{\mathrm{fcc}}_{\mathrm{Al:Al:Al:Fe}} &= 3u_{\mathrm{AlFe}} + 9000 \\
{}^{o}G^{\mathrm{fcc}}_{\mathrm{Al:Al:Fe:Fe}} &= 4u_{\mathrm{AlFe}} \\
{}^{o}G^{\mathrm{fcc}}_{\mathrm{Al:Fe:Fe:Fe}} &= 3u_{\mathrm{AlFe}} - 4000.
\end{aligned}
\tag{8}
$$

The values of the excess parameters in Eq. (5), the bond energy u_{AlFe} and the ordered end member parameters were fitted to the *ab initio* data in Table 1, the *ab initio* calculated energies for the disordered fcc phase in Table 2 and the tie-lines between fcc and bcc at 1473 K, see Fig. 2(b). In the same assessment the information from the stable Al–Fe phase diagram i.e. the γ-loop on the Fe-rich side and the experimental data on the solubility of Fe in fcc-Al were also fitted.

The changes of the γ-loop and solubility of Fe in Al are shown in Fig. 3. The new γ-loop is compared with the previous assessment of Seiersten [19] which is plotted with dashed lines and experimental information. The experimental data on the solubility of Fe in fcc-Al is shown in Fig. 3(b) together with the calculated solubility line. This solubility is very critical as Fe is an important impurity in aluminium alloys.

The assessed metastable-ordered fcc phase diagram is shown in Fig. 3(c). The stability at higher temperatures is limited by the fact that the fcc phase and its ordered forms must not become stable relative to bcc. On the Al-rich side the $L1_2$-ordered phase is metastable even relative to disordered fcc. The *ab initio* calculations of the disordered fcc and bcc phases and the assessed values for different compositions are listed in Table 2. The agreement between the values is reasonable.

3. Thermodynamic models

All models used are based on the Compound Energy Formalism (CEF), this uses the point approximation for the configurational entropy of mixing and sublattices to describe long-range order. Except for the $E2_1$ phase these models have been used many times in published assessments and only a brief summary of the equations is given here.

3.1. The liquid phase

The liquid phase is modelled with a substitutional regular solution model using Redlich–Kister series for the excess Gibbs energy.

$$G_m = \sum_i x_i \, {}^oG_i + RT \sum_i x_i \ln(x_i) + {}^EG_m \tag{9}$$

where x_i are the mole fraction of components i and ${}^oG_i$ are the Gibbs energies of the components in the liquid state relative to the SER (Stable Element Reference) state, the stable state at 298.15 K and 1 bar. Functions for these Gibbs energies for the liquid and other phases are taken from SGTE [15].

The term multiplied with RT, where R is the gas constant and T the absolute temperature, is the configurational entropy and ${}^EG_m$ is the excess Gibbs energy taking into account both binary and ternary interactions

$${}^EG_m = \sum_i \sum_{j>i} x_i x_j \left(L_{ij} + \sum_{k>j} x_k L_{ijk} \right). \tag{10}$$

The binary interaction parameters can be composition dependent using a Redlich–Kister series

$$L_{ij} = \sum_{\nu=0}^{n} (x_i - x_j)^\nu \, {}^\nu L_{ij} \, . \tag{11}$$

3.2. The bcc phase with B2 ordering

The B2 ordering in Al–Fe is a second-order transformation from the disordered bcc phase (A2) and one must thus have the same Gibbs energy function for both A2 and B2. To describe the B2 ordering the substitutional sublattice is divided into two identical sublattices and one must take into account that there are both anti-site defects and vacancy defects (structural vacancies) in the B2 lattices. The phase will be called B2 also when there is interstitial carbon in the phase. As there are 3 times as many interstitial sites as there are substitutional the model for B2 is:

$$(\mathrm{Al, Fe, Va})_{0.5}(\mathrm{Al, Fe, Va})_{0.5}(\mathrm{Va, C})_3. \tag{12}$$

The fraction of the constituents on each sublattice is denoted by the constituent fraction $y_i^{(s)}$ where s is the sublattice and i is the constituent. The mole fraction of a component can be calculated by summing the content of this component over all sublattices excluding the vacancies:

$$x_i = \frac{\sum_s a_s y_i^{(s)}}{\sum_s a_s (1 - y_{\mathrm{Va}}^{(s)})}. \tag{13}$$

The contribution to the Gibbs energy due to the ferromagnetic transition, ${}^{\mathrm{magn}}G_m$ is described with a phenomenological model proposed by Inden [10] as a function of the Curie temperature and the Bohr magneton number, both of which can be composition dependent. The Gibbs energy function for the A2 and B2 phases is

$$G_m = \sum_i \sum_j \sum_k y_i^{(1)} y_j^{(2)} y_k^{(3)} \, {}^oG_{ijk} + RT \sum_s a_s \sum_i y_i^{(s)} \ln(y_i^{(s)}) + {}^{\mathrm{magn}}G_m + {}^EG_m \, . \tag{14}$$

The ${}^oG_{ijk}$ parameters represent the Gibbs energy of formation of a compound with a single constituent in each sublattice within the solution phase. The term multiplied with RT is the configurational entropy as a sum of the ideal mixing in each sublattice separately weighted by the number of sites, a_s.

The excess Gibbs energy, ${}^EG_m$, includes terms representing interaction between constituents on each sublattice and also simultaneous interaction between constituents on different sublattices. Explanations of this and the ${}^{\mathrm{magn}}G_m$ terms can be found in in the book by Lukas et al. [34] together with a detailed discussion of the ordering model.

3.3. Partitioning of the Gibbs energy

The model in Eq. (14) can describe both the ordered B2 and the disordered A2, in the latter case the site fractions on the substitutional sublattices are identical and equal to the mole fractions:

$$y_i^{(1)} = y_i^{(2)} = x_i. \tag{15}$$

But as there are many systems with a bcc phase without B2 ordering it is convenient, when developing multicomponent databases, that one separates the "disordered" part of the Gibbs energy function that can be described with the model

$$(\mathrm{Al, Fe, Va})_1(\mathrm{Va, C})_3 \tag{16}$$

from the ordered part and writes the Gibbs energy as a sum of two parts:

$$G_m = G_m^{\mathrm{dis}}(x_i) + \Delta G_m^{\mathrm{ord}}(y_i) \tag{17}$$

$$\Delta G_m^{\mathrm{ord}} = G_m^{\mathrm{ord}}(y_i) - G_m^{\mathrm{ord}}(y_i = x_i). \tag{18}$$

The disordered part describes the whole Gibbs energy when the phase is disordered, i.e. when Eq. (15) applies. $\Delta G_m^{\mathrm{ord}}$ must thus be zero when the phase is disordered and this is achieved in Eq. (18) by calculating the same Gibbs energy function twice, once with the original site fractions and once with the site fractions set equal to their disordered values.

The function G_m^{ord} thus contains parameters related to ordering only. Note that the interstitial sublattice is not affected by the order/disorder transition and all parameters for the interstitial constituents should be given in the disordered part.

3.4. Restricting the thermal vacancies

The model for B2 has structural vacancies in the substitutional sublattices. In Al–Fe system the fraction of such vacancies is very small up to equiatomic composition and then the B2 phase is no longer stable. However, in systems like Al–Ni the vacancy fraction in the B2 phase is very important and thus they must be included in the model for any B2 phase

(and subsequently the A2 phase) which should be compatible with the Al–Ni system. In the A2 phase these vacancies have the same function as thermal vacancies but those are normally not included in the modelling. In order to keep the fraction of these vacancies very low the following parameter is recommended

$$^{o}G^{\mathrm{A2}}_{\mathrm{Va:Va}} = 30T. \quad (19)$$

This parameter ensures that there will never be any significant fraction of thermal vacancies in the A2 phase. In the B2 phase one may assess parameters like $L^{\mathrm{B2}}_{i,\mathrm{Va:Va:Va}} = L^{\mathrm{B2}}_{\mathrm{Va:}i,\mathrm{Va:Va}}$ to describe the structural vacancies as has been done for the Al–Ni system by Dupin [26].

3.5. The fcc phase and its ordered forms

The fcc phase, Structurbericht A1, with an octahedral interstitial sublattice for carbon has a B1 structure with a high amount of vacancy defects in the interstitial sublattice. There are other systems, for example Ti–C, with a B1 structure with lower fraction of vacancies but for simplicity the fcc phase with a small fraction of interstitial carbon can be denoted A1.

There are many types of ordering based on the fcc lattice but the most important cases are the $L1_2$ and $L1_0$ ordering which can be modelled with 4 substitutional sublattices with equal number of sites. Adding the interstitial sublattice the model is

$$(\mathrm{Al, Fe})_{0.25}(\mathrm{Al, Fe})_{0.25}(\mathrm{Al, Fe})_{0.25}(\mathrm{Al, Fe})_{0.25}(\mathrm{Va, C})_1. \quad (20)$$

As described for the A2 and B2 phases the Gibbs energy for this phase is usually partitioned into a disordered fcc phase with one substitutional and one interstitial sublattice and an ordered part with four substitutional sublattices for the metallic components and one interstitial. The disordered model is:

$$(\mathrm{Al, Fe})_1(\mathrm{Va, C})_1. \quad (21)$$

The Gibbs energy expressions are similar for the fcc-ordered phase as for the B2 given in Eq. (14) except that there are five sublattices instead of three. The fcc phase is disordered when it has the same fractions on all four substitutional sublattices.

Both the disordered fcc phase and the ordered phases formed from the fcc lattice will be described with the same Gibbs energy function and it will be denoted fcc unless the ordering is important.

In the fcc phase sro is much more important than in the A2 phase. An approximation of this sro for CEF was derived by Sundman and Mohri [17].

3.6. The κ phase

The κ carbide with Structurberict $E2_1$, has ordering both on the substitutional and the interstitial sublattices. On the metallic sublattices one has an $L1_2$ ordering with Fe on the cube surfaces and Al at the cube corners. On the interstitial sublattice carbon prefers the octahedral site in the middle of the cube where it has only Fe atoms as nearest neighbours, i.e. 1/4 of the available sites. As the interstitial sublattice is an fcc lattice this is in principle an $L1_2$ ordering of carbon and vacancies.

It is possible to model the $E2_1$ as an ordered fcc phase with 4 sublattices for the metallic components and 4 for the interstitial. However, this would give 8 sublattices with $2^8 = 256$ end members and although many of them are identical such a complex model is outside the scope of this paper. The necessary simplification will be to assume that there is only vacancies in the 3 interstitial sublattices that should be empty in the $E2_1$ structure but there may be vacancies in the remaining one. This means that the κ phase will be described with the following model:

$$(\mathrm{Al, Fe})_{0.25}(\mathrm{Al, Fe})_{0.25}(\mathrm{Al, Fe})_{0.25}(\mathrm{Al, Fe})_{0.25}(\mathrm{Va, C})_{0.25}. \quad (22)$$

Without any interstitial carbon this model is identical to the fcc phase with ordering described for the binary Al–Fe system in Section 2.2 and the corresponding parameters for the κ phase are copied from the fcc phase. As carbon enters only in 1/4 of the interstitial sites that is available in the disordered fcc phase according to Eq. (20), the values for the end member parameters $^{o}G^{\mathrm{E2_1}}_{\mathrm{Fe:Fe:Fe:Fe:C}}$ and $^{o}G^{\mathrm{E2_1}}_{\mathrm{Al:Al:Al:Al:C}}$ are approximated by the values of the Gibbs energy of the fcc phase at these compositions according to Eq. (25). The maximum solubility of C with this model is 20 at.% which is well outside the stable range of the phase.

The parameters for the ordered $E2_1$ phase with the interstitial sublattice filled with carbon can be fitted to experimental solubilities and *ab initio* data. In the model for the $E2_1$ phase its Gibbs energy is partitioned into an ordered and disordered phase as for fcc and bcc phases, Eq. (17). When extrapolating to higher-order systems one can take advantage of the fact that the $E2_1$ phase has a similar model to fcc and copy known fcc parameters to the $E2_1$ model and obtain reasonable fit to experimental data with no or few additional parameters.

4. Experimental data and results of the optimization

The experimental work by Palm and Inden [20] at three temperatures, 1073, 1273 and 1473 K was the main information used in addition to their experimental information for the liquidus. The experimental data was used to fit ternary parameters in liquid, fcc and κ phase.

The calculated isothermal phase diagrams at 1073 K, 1273 K and 1473 K are shown in Fig. 4(a)–(c) and the liquidus lines in Fig. 4(d). Considering the scattering and possible inaccuracies in the experimental information, the overall fit obtained is satisfactory. At 1073 and 1273 K there is no two-phase region between bcc and graphite on the Al-rich side of the κ phase as found experimentally. It would be possible to modify the stability of the Al_4C_3 carbide slightly to obtain a 3-phase region bcc + κ + graphite but such a change was considered outside the scope of this assessment. At 1273 K the two-phase region fcc+bcc is more narrow than the experimental one but to obtain a better fit for this region the solubility line for graphite in fcc should be shifted to higher carbon content and this would lead to too high solubility at 1473 K. The κ phase region is smaller than experimentally found at both 1273 and 1473 K and extends a bit too much towards the binary Al–Fe side at 1073 K.

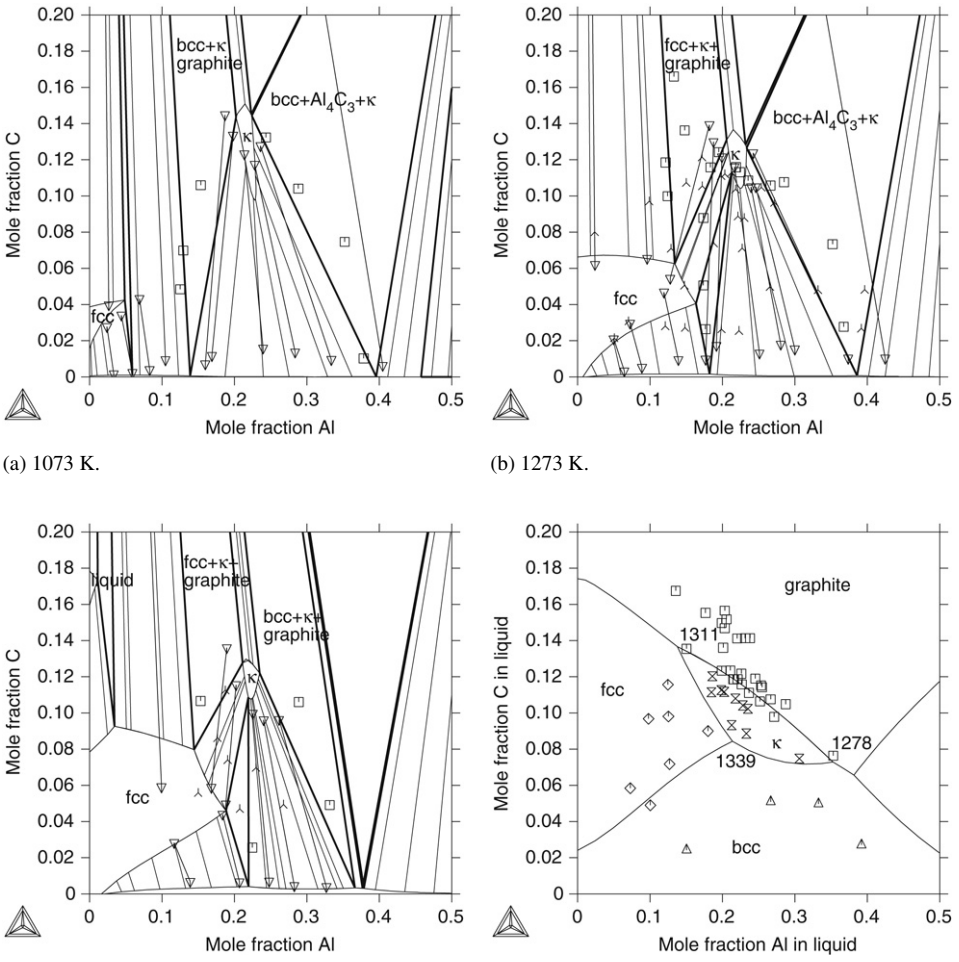

(a) 1073 K.

(b) 1273 K.

(c) 1473 K.

(d) Monovariant liquidus lines.

Fig. 4. Calculated isothermal sections and the monovariant liquidus lines. For the isothermal sections experimental data from [20] are shown, tie-lines are delimited by ▽ symbols, two-phase regions are denoted by the symbol ϒ and three-phase regions by □. In (d) the first solid phase found experimentally is denoted by ◇ for fcc, △ for bcc, □ for graphite and ⧖ for the κ phase.

At 1073 and 1273 K the calculated solubility of C in bcc is much smaller than the experimental data but it would require a significant change in the model parameters for the bcc to accommodate such a high solubility, in particular since the solubility seems to decrease with increasing temperature. It should be interesting to have further experimental work on this.

The calculated monovariant lines of the liquid in equilibrium with two solid phases are shown in Fig. 4(d). For the liquidus surface the different symbols show the first solid phase at various compositions from Palm and Inden [20]. The temperatures in degree Celsius at the invariant four-phase equilibria are shown in the diagram and in Table 3 there is a comparison with other assessments of the temperatures for the invariants.

Palm and Inden [20] assessed also two isopleths for fixed contents of C and one for a fixed content of Al. Similar sections have been calculated and are shown in Fig. 5(a)–(c) together with experimental information. The general agreement between the assessed and calculated isopleth sections is very good. One has to take into account that the lines in these diagrams can shift significantly with a very small amount of the phases present. In the present assessment the Al_4C_3 phase is in equilibrium with the κ phase at low temperatures and thus there are some additional calculated lines compared to the diagram by Palm and Inden [20].

4.1. Assessed parameters

As the data involving the liquid is for a very small temperature range a single temperature-independent parameter was used and its final value was:

$$L^{\mathrm{liq}}_{\mathrm{Al,C,Fe}} = -49\,000. \tag{23}$$

For the disordered fcc phase two parameters were used, the regular solution parameters for Al and Fe with the interstitial sublattice filled with C. Their final values were

$$\begin{aligned} {}^{0}L^{\mathrm{fcc}}_{\mathrm{Al,Fe:C}} &= -104\,000 + 80T \\ {}^{1}L^{\mathrm{fcc}}_{\mathrm{Al,Fe:C}} &= 81\,000. \end{aligned} \tag{24}$$

Adding more parameters did not significantly improve the fit and it became very difficult to restrict the parameter values within reasonable limits as there were so few experimental points.

Table 3
Calculated temperatures in °C for the invariant equilibria with the liquid compared with assessed values from other authors

Phases	This work	[28]	[20]	[16]	[12]
liquid + fcc + bcc + κ	1339	1342	1315	1318	1313
liquid + bcc + graphite + κ	1278	1308	1295	1297	1305
liquid + fcc + graphite + κ	1311	1365	1282	1282	1284

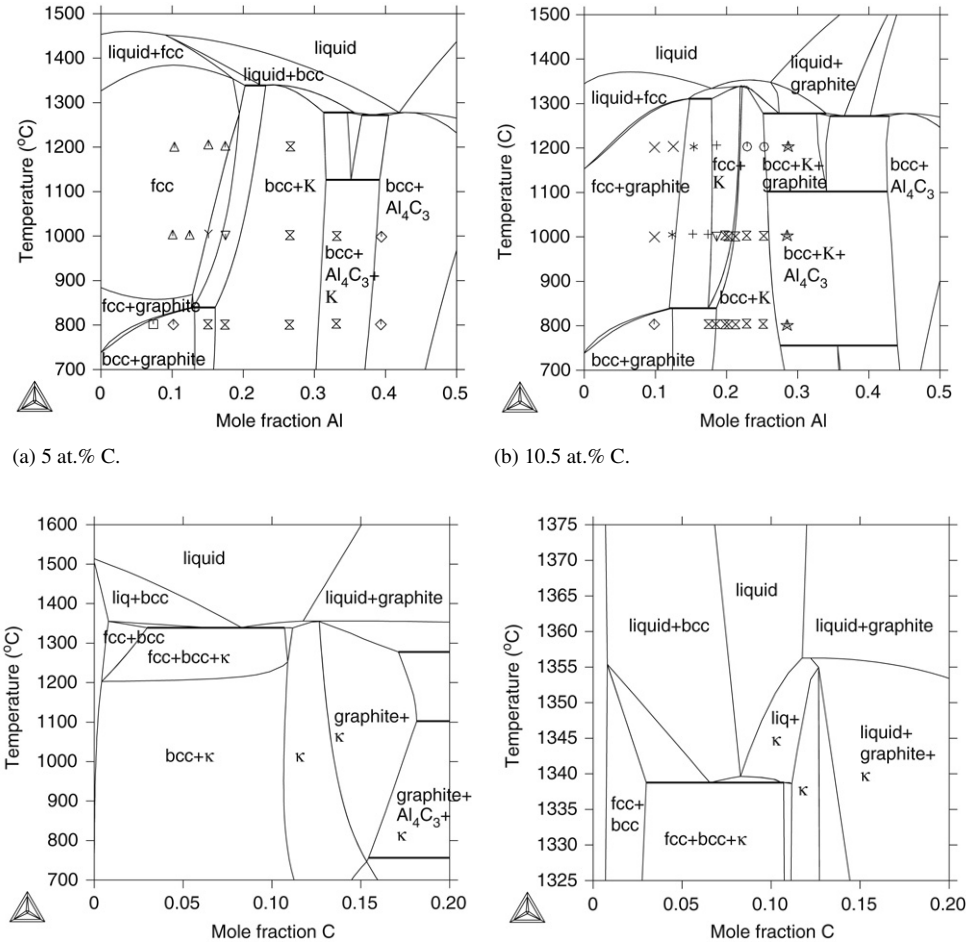

(a) 5 at.% C.

(b) 10.5 at.% C.

(c) 22 at.% Al.

(d) Magnification of 22 at.% Al.

Fig. 5. Isopleth calculations for two fixed carbon compositions and one fixed Al composition. The symbols are experimental data by [20] and the single phase regions are denoted △ for fcc and ○ for κ, two-phase regions ϒ for fcc + bcc, × for fcc + graphite, + for fcc + κ, ◇ for bcc + graphite, ⧖ for bcc + κ and the three-phase regions □ for fcc + bcc + graphite, ▽ for fcc + bcc + κ, ∗ for fcc + graphite + κ and ⋆ for bcc + graphite + κ. The magnified section for 22 at.% Al shows the phase regions around the invariant liquid + fcc + bcc + κ reaction at 1339 °C.

For the κ phase the parameters for the binary Al–Fe are almost identical to the fcc phase as described above. The end members $AlC_{0.25}$ and $FeC_{0.25}$ were set equal to the Gibbs energy of the fcc phase at $x_C = 0.2$ i.e. $y_C = 0.25$ using the following formula where M is either Al or Fe:

$$
\begin{aligned}
&{}^{o}G^{\kappa}_{\mathrm{M:C}} - {}^{o}G^{\mathrm{fcc}}_{\mathrm{M}} - 0.25\,{}^{o}G^{\mathrm{graphite}}_{\mathrm{C}} \\
&= 0.25({}^{o}G^{\mathrm{fcc}}_{\mathrm{M:C}} - {}^{o}G^{\mathrm{fcc}}_{\mathrm{M}} - {}^{o}G^{\mathrm{graphite}}_{\mathrm{C}}) \\
&\quad + 0.75({}^{o}G^{\mathrm{fcc}}_{\mathrm{M:Va}} - {}^{o}G_{\mathrm{M}}) + RT(0.25\ln(0.25) \\
&\quad + 0.75\ln(0.75)) + 0.25\cdot 0.75\cdot L^{\mathrm{fcc}}_{\mathrm{M:C,Va}}. \qquad (25)
\end{aligned}
$$

Note that the parameter ${}^{o}G^{\kappa}_{\mathrm{M:C}}$ is for 1.25 moles of atoms. The finally assessed parameters for the disordered kappa, those without carbon copied from the fcc phase in Al–Fe, are

$$
{}^{o}G_{\mathrm{Al:C}} - {}^{o}G^{\mathrm{fcc}}_{\mathrm{Al}} - 0.25\,{}^{o}G^{\mathrm{graphite}}_{\mathrm{C}} = 5250 - 3.1755T \qquad (26)
$$

$$
{}^{o}G_{\mathrm{Fe:C}} - {}^{o}G^{\mathrm{fcc}}_{\mathrm{Fe}} - 0.25\,{}^{o}G^{\mathrm{graphite}}_{\mathrm{C}} = 12\,801 - 8.3655T \qquad (27)
$$

$$
{}^{o}G_{\mathrm{Al:Va}} - {}^{o}G^{\mathrm{fcc}}_{\mathrm{Al}} = 100 \qquad (28)
$$

$$
{}^{o}G_{\mathrm{Fe:Va}} - {}^{o}G^{\mathrm{fcc}}_{\mathrm{Fe}} = 100 \qquad (29)
$$

$$
L_{\mathrm{Fe:C,Va}} = 2000 \qquad (30)
$$

$$
{}^{0}L_{\mathrm{Al,Fe:Va}} = {}^{0}L^{\mathrm{fcc}}_{\mathrm{Al,Fe:Va}} = -104\,700 + 30.65T \qquad (31)
$$

$$
{}^{1}L_{\mathrm{Al,Fe:Va}} = {}^{1}L^{\mathrm{fcc}}_{\mathrm{Al,Fe:Va}} = 22\,600 \qquad (32)
$$

$$
{}^{2}L_{\mathrm{Al,Fe:Va}} = {}^{2}L^{\mathrm{fcc}}_{\mathrm{Al,Fe:Va}} = 29\,100 - 13T \qquad (33)
$$

Table 4
The *ab initio* calculated values for the ordered $E2_1$ (κ) phase at various compositions together with the corresponding values from the Calphad assessment

Mole fractions			E_f	E_f	Reference
Al	C	Fe	(meV/atom)	(kJ/mol atom)	(kJ/mol atom)
0.8	0.2	0	304	29.4	[36]
0.8	0.2	0	–	4.2	Assessed this work
0.6	0.2	0.2	331	32.0	[36]
0.6	0.2	0.2	–	−7.4	Assessed this work
0.2	0.2	0.6	–	−27.9	[28]
0.2	0.2	0.6	−188	−18.4	[36]
0.2	0.2	0.6	–	−16.0	Assessed this work
0	0.2	0.8	93	9.0	[36]
0	0.2	0.8	–	16.7	Assessed this work

$$^{0}L_{\mathrm{Al,Fe:C}} = -149\,000 + 86T \tag{34}$$

$$^{1}L_{\mathrm{Al,Fe:C}} = 99\,000 - 48T \tag{35}$$

$$L_{\mathrm{Al,Fe:C,Va}} = 74\,200 - 77T. \tag{36}$$

The end member parameters for pure Al and Fe in Eqs. (28) and (29) are set 100 J/mol higher than the corresponding for the fcc phase to emphasize the similarity but to avoid that the κ phase becomes stable in the binary Al–Fe system. The temperature dependence may seem rather high but the ratio between "enthalpy" and "entropy" parts of the parameters is around 1000 or larger which is quite normal. However, one must be careful that the values obtained do not lead to unreasonable extrapolations at low or high temperatures.

The assessed parameters for the ordered end members with carbon are

$$u_{\mathrm{AlFeC}} = -1600 - 16.8T \tag{37}$$

$$^{o}G_{\mathrm{Al:Fe:Fe:C}} = 3u_{\mathrm{AlFeC}} \tag{38}$$

$$^{o}G_{\mathrm{Al:Al:Fe:C}} = 4u_{\mathrm{AlFeC}} - 5200 \tag{39}$$

$$^{o}G_{\mathrm{Al:Al:Al:C}} = 3u_{\mathrm{AlFeC}} \tag{40}$$

$$L_{\mathrm{Al,Fe:Al,Fe:*:C}} = L_{\mathrm{Al,Fe:*:Al,Fe:*:C}} = \cdots = u_{\mathrm{AlFeC}}, \tag{41}$$

where u_{AlFeC} is the average bond energy between Al and Fe in the fcc tetrahedra with a carbon atom in the central octahedral site. The asterisk "*" in a sublattice means that the parameter is independent of the constituent in that sublattice. The end member value for the Al_3FeC compound could not be fitted to the *ab initio* value in Table 4 as that made it difficult to describe the stable range of the κ phase, instead it was assumed to be the same as that for the stable $AlFe_3C$ end member. The end member values for Fe_4C and Al_4C for the κ phase was set similar to the disordered fcc phase at 20 at.% C from the already assessed C–Fe and Al–C binaries as given by Eq. (25).

Several other parameters were allowed to vary during the optimization but none of them had a significant influence and they were finally set to zero.

There is no information how far below 1073 K the κ phase is stable and without this information the assessment gave that the κ phase became unstable around 800 K. That is not impossible because graphite has difficulties both to nucleate and to grow but a fictitious experimental point was added that the κ should be stable at least at 500 K. This did not change the assessed parameters significantly but made the κ phase stable down to 0 K.

The metastable phase diagrams for the disordered and different ordered forms of the κ phase at 973 and 1273 K are shown in Fig. 6. In addition to the stable Fe_3AlC phase there are also metastable-ordered phases at the compositions Al_2Fe_2C and Al_3FeC respectively with varying carbon content. As the κ phase is almost identical to the fcc phase along the Al–Fe binary it is interesting to note that the κ phase joins with the metastable-ordered $L1_2$ on the Al–Fe binary at 973 K. Also, there is a miscibility gap in the fcc phase on the Al-rich side at 973 K.

5. Summary

The Al–C–Fe ternary system has been assessed using both *ab initio* data and experimental information on the phase diagram. The extrapolation of the fcc and bcc phases from the binaries into the ternary system indicated that the relative stability of the bcc and fcc phases was not correct, see Fig. 2, and could not be corrected by any ternary parameters. Thus a reassessment of Al–C and Al–Fe was made with minimal changes of the stable binary descriptions. Other extrapolations from the new binary Al–Fe were also checked, for example into the Al–Fe–Ni system. With the original Al–Fe system the extrapolation into the ternary fitted well experimental data without any ternary parameters. With the modified Al–Fe binary a small positive ternary parameter in the fcc phase was needed to have the same good fit but this was considered acceptable. In the Al–Fe–Mn system a previously negative ternary interaction in fcc could be set to zero to obtain a reasonable ternary phase diagram.

Whenever *ab initio* data is used to describe metastable ordering, like here for the fcc phase in Al–Fe, it is important to assess a reasonable description for all possible ordered forms allowed by the model, not just the one currently important, because the binary is used in many different ternary assessments and one cannot revise it too many times. But there is still a need to reassess the stable Al–Fe binary to fit the $D0_3$ ordering using 4 sublattices also for the bcc phase for example to extrapolate into the Al–Fe–Ti system.

As already mentioned the solubility of carbon in the Al-rich bcc phase needs to be confirmed by new experimental work. The complete set of parameters for this system can be obtained as a TDB file from the website http://www.mse.kth.se/~bosse.

Acknowledgements

Computer resources for this job were provided by CALMIP (Toulouse, France) and the computer center GRID'5000 Nation-Wide Grid Experimental platform funded by the French Ministery of Research through the ACI GRID program. INRIA, CNRS and RENATER and other contributing partners (see https://www.grid5000.fr) GRID5000 France. One of the authors, BS, is grateful for a senior research grant from CNRS.

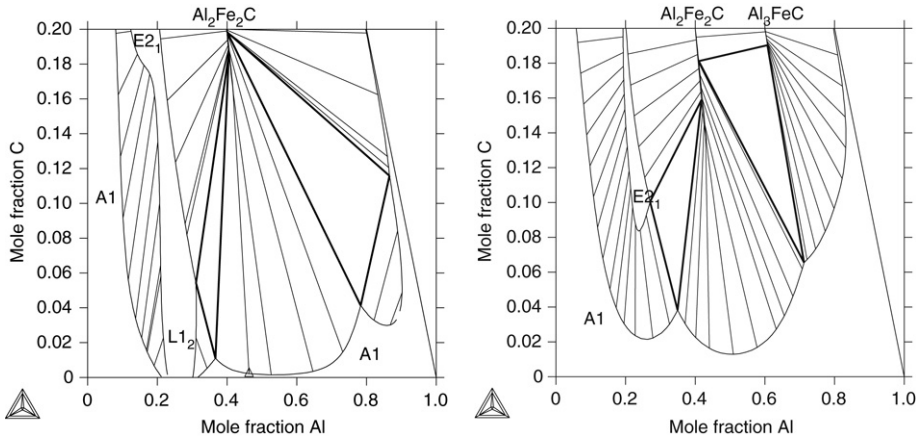

(a) 973 K. (b) 1273 K.

Fig. 6. Isothermal metastable sections at two temperatures with only κ and A1.

Appendix. First principle methodology

Full details of the calculations reported here can be found in Connetable et al. [36]. The *ab initio* approach is based on the Density Function Theory (DFT) developed by Hohenberg and Kohn [7,5]. The Perdew–Burke–Ernzerhof (PBE) [22] generalized gradient approximation (GGA) has been employed for the exchange and correlation functional in its spin-polarized version. The Vienna *ab initio* simulation package *VASP* developped by the Hafner's group [18], implementing the projector augmented wave (PAW) method [24] was used.

Brillouin-zone sampling was performed using the Monkhorst-Pack scheme [9] with a $20 \times 20 \times 20$ mesh grid centered on the **k**-point. For the phases, the plane-wave energy cutoff is 600 eV. The ion relaxations and cell relaxations were performed using the standard conjugate gradient algorithms implemented in the *VASP* code. The forces are fully relaxed with a criterion for stopping the structural optimization of 0.05 eV/Å. The chosen energy cutoff, **k**-points and convergence parameters were checked to ensure a convergence in energy of the order of 1 meV per atom.

The formation enthalpies at 0 K are calculated taking as reference the following pure phases: Fe in the bcc ferromagnetic state, Al in the fcc state, and C in the diamond state. The convention that the formation enthalpy is negative for a stable phase and positive in the opposite case was used. Enthalpies are given either in kJ per mole of atoms either in meV per atoms.

To simulate disordered Fe_xAl_{1-x} binaries the SQS ('Special Quasirandom Structures') framework as proposed by A. Zunger [14] was employed. In this formalism the fcc and bcc Fe_xAl_{1-x} random binary compounds for different values of x was studied. The structures proposed by Jiang et al. [27] was used for the bcc structure ($x = 0.25$, and $x = 0.75$) and the SQS structures given by Sluiter [32] for fcc structures ($x = 1/6$, 0.25, $1/3$ and 0.5).

References

[1] M. Isawa, T. Murakamim, Kinsoku-no-Kenkyu 4 (1927) 467.
[2] F. Wever, A. Muller, Zeitsch. Anorg. Chem. 192 (1930) 340.
[3] I.K. Edgar, Trans. AIME 180 (1948) 225.
[4] C. Crussard, F. Aubertin, Rev. Metal XLVI (1949) 661.
[5] W. Kohn, Phys. Rev. Lett. 2 (1959) 393;
W. Kohn, L.J. Sham, Phys. Rev. 140 (1965) A1133.
[6] A.G. Lisnik, V.P. Skvorchuk, Dopovidi Akad. Nauk. Ukr. RSR (1960).
[7] P. Hohenberg, W. Kohn, Phys. Rev. 136 (1964) B864.
[8] K. Anderko, F.A. Shunk, Constitution of Binary Alloys, Suppl. 2, McGraw-Hill, NY, ISBN: 9970034375, 1969.
[9] H.J. Monkhorst, J.D. Pack, Phys. Rev. B 13 (1976) 5188.
[10] G. Inden, Physica 103B (1981) 82.
[11] P. Gustafson, Scan. J. Metall. 14 (1985) 259.
[12] E. Schürman, J. Schweinichen, Giessereiforschung 38 (1986) 125.
[13] A. Oscarsson, W.B. Hutchinson, H.-E. Ekström, D.P.E. Dickson, C.J. Simensen, G.M. Raynaud, Z. Metallkde 79 (1988) 600.
[14] A. Zunger, S.-H. Wei, L.G. Ferreira, J.E. Bernard, Phys. Rev. Lett. 65 (1990) 353.
[15] A.T. Dinsdale, CALPHAD 15 (1991) 317.
[16] H.K.C. Kumar, V. Raghavan, J. Phase Equil. 12 (1991) 275.
[17] B. Sundman, T. Mohri, Z. Metallkde 81 (1990) 251.
[18] G. Kresse, J. Hafner, Phys. Rev. B 47 (1993) 558; 49 (1994) 14251;
G. Kresse, J. Furthmüller, Phys. Rev. B 54 (1996) 11169;
G. Kresse, J. Furthmüller, Comput. Mater. Sci. 6 (1996) 15.
[19] M. Seiersten, SINTEF report STF-28F93051, Oslo, Norway, 1993.
[20] M. Palm, G. Inden, Intermetallics 3 (1995) 443.
[21] J. Gröbner, H.L. Lukas, F. Aldinger, CALPHAD 20 (1996) 247.
[22] J.P. Perdew, K. Burke, M. Ernzerhof, Phys. Rev. Lett. 77 (1996) 3865. 78 (1997) 1396.
[23] R.E. Watson, M. Wienert, Phys. Rev. B 58B (1998) 5981.
[24] G. Kresse, D. Joubert, Phys. Rev. B 59 (1999) 1758;
P.E. Blöchl, Phys. Rev. B 50 (1994) 17953.
[25] I. Ohnuma, private communication 2000.
[26] N. Dupin, I. Ansara, B. Sundman, CALPHAD 25 (2001) 279.
[27] C. Jiang, C. Wolverton, J. Sofo, L.-Q. Chen, Z.-K. Liu, Phys. Rev. B 69 (2004) 214202.
[28] H. Ohtani, M. Yamano, M. Hasebe, ISIJ Int. 44 (2004) 1738.
[29] T. Abe, B. Sundman, CALPHAD 27 (2003) 403.
[30] F. Lecherman, M. Fähnle, J.M. Sanchez, Intermetallics 13 (2005) 1096.
[31] H.L. Skriver, http://databases.fysik.dtu.dk.
[32] M. Sluiter, private communications.
[33] M. Widom, http://alloy.phys.cmu.edu.
[34] H.L. Lukas, S.G. Fries, B. Sundman, Computational Thermodynamics, Cambridge Univ. Press, Cambridge UK, ISBN: 9780521868112, 2007.
[35] TCFE5, thermodynamic steel database. http://www.thermocalc.se, 2007.
[36] D. Connetable, to be published.
[37] P.E.A.,Turchi, et al., CALPHAD 31 (2007) 4.